Application of the incubation time criterion for dynamic brittle fracture

A. Dorogoy*, A. Godinger and D. Rittel
Faculty of Mechanical Engineering, Technion – Israel Institute of Technology, 32000, Haifa, Israel.

Abstract

The complex issue of penetration and perforation of brittle plates subjected to normal impact is addressed. Fracture and fragmentation are simulated numerically by using simultaneously two failure criteria: ductile and brittle failure. A new brittle failure criterion, which is based on incubation time is proposed. The criterion, inspired from the Tuler-Butcher criterion, is implemented in a commercial finite element code by means of a user subroutine. It is validated by comparing numerical predictions to experimental ballistic results of normal impact on polymethylmethacrylate plates. It is shown that the projectile's exit velocity and the timing of the penetration are faithfully reproduced. It is also verified visually that the experimental damage/fracture pattern, namely radial cracking and dishing, are both well captured by the proposed criterion.

Key words: incubation time, brittle fracture, polymethylmethacrylate, dynamic fracture, finite element

(*) A. Dorogoy, corresponding author: *dorogoy@technion.ac.il*

1. Introduction

Modelling dynamic brittle fragmentation (e.g. as the result of ballistic impact) is a delicate issue for its complexity. The physical phenomena governing the fragmentation and the projectile-target interaction are not straightforward [1]. Various published numerical models are based on different approaches, such as cohesive elements [2]–[4], meshless methods [5], [6], smooth particle hydrodynamics [7] (SPH), or peridynamics [8], [9]. All those methods are aimed at modeling the dynamic fragmentation process in itself, while the material models are assumed to be identified separately, the most popular material models being that of Johnson-Cook [10], [11] or Johnson-Holmquist [12]–[15].

Each of those methods and the associated material models have their respective merits and success in describing ballistic perforation [4], [16]–[19] or brittle fracture [2], [4], [20]–[24] [25]–[31], but one of the drawbacks can be the lack of extensive experimental validation coupled to a sometimes excessive level of complexity, that renders the straightforward application of those approaches delicate for common engineering problems.

However, if the physics of fragmentation can be somewhat deepened, there is a reasonable chance that the numerical models be simplified accordingly. Among the main physical mechanisms of interest in brittle fragmentation, one can identify the nature of the dynamic interaction between multiple cracks and defects, all developing almost simultaneously. In essence, while a single defect may dominate the process under quasi-static loading, brittle dynamic fragmentation involves a multitude of microdefects that interact with each other. Hild et al. [32], [33] resorted to statistical descriptions of this interaction with mutual shielding effects between defects. This approach has its merit although the assumption of a weakest link statistics governing the dynamic fragmentation may be questionable [24].

Many years ago, Kalthoff and Shockey [34] showed that for a defect to propagate under impulsive loading, a certain duration must elapse during which the critical stress threshold is exceeded otherwise there is no defect growth, introducing what is now known as the “incubation time".

Dynamic fracture experiments reveal a fundamental difference between the fast dynamic rupture (breakdown) of materials and a similar process under slow quasi static loading. This difference was addressed by some non-classical approaches and development of a new criteria for brittle fracture, as described in Morozov and Petrov and Bratov's books [35], [36]. One early time-dependent criterion for general dynamic fracture was introduced by Tuler and Butcher [37], and was used successfully to calculate spall layer thicknesses in aluminum. The criterion has the form $\int_0^{t_f} \left(\sigma\left(t'\right)-\sigma_0\right)^{\lambda} dt' = K$ where λ and K are constants and $\sigma\left(t'\right)$ is tensile stress and σ_0 is a limit tensile stress below which fracture would not occur. Morozov and Petrov [35] proposed a structure–time criterion that takes into account the time variation of the load and the material. In the case of "flawless" media, it has the form $\int_{t-\tau}^{t} \sigma\left(t'\right) dt' = \sigma_c \tau$, where τ is the incubation (material/structural) time of fracture, namely the shortest possible time needed for a load exceeding some threshold value to create rupture. A unified interpretation [38] which uses the concept of the fracture incubation time was subsequently developed [39], [40] .

In this work, we assume a threshold principal stress criterion that triggers damage accumulation. The proposed criterion is implemented in a commercial finite element code [41] by means of a user subroutine [42]. Validation is achieved by comparing numerical predictions to experimental ballistic results of normal impact on polymethylmethacrylate (PMMA) plates. It is shown that a quantitative reproduction of the projectile's exit velocity and the timing of the penetration are faithfully reproduced. It is also verified visually that the experimental damage/fracture pattern, namely radial cracking and dishing, are both well captured by the proposed criterion.

The paper is organized as follows: After this introduction, the criterion is presented in section 2. Section 3 details the numerical procedure while section 4 describes the experimental set up and velocity results. The experimental and numerical results are compared in section 5, followed by a summary and conclusions in section 6.

2. *Fragmentation criterion based on incubation time*

In this section we first introduce the new brittle fracture criterion followed by a short discussion of the differences between this criterion and previous similar criteria. It is shown that the new criterion can also be derived from the kinetic equation of damage.

2.1 The criterion

We assume that damage at a material point will start to accumulate if this point has endured a threshold tensile principal stress denoted $\sigma_I^{treshold}$. Once a material point experiences $\sigma_I^{treshold}$ at time t = t*, damage accumulates for all t > t* if $\sigma_m(t) > 0$, where $\sigma_m = \frac{\sigma_{ii}}{3}$, $i = 1 \cdots 3$ is defined as the hydrostatic stress. The accumulation of damage is related to the parameter D_a of Eqn. 1:

$$D_a = \int_{t^*}^{t} \sigma_m\left(t'\right) dt' \qquad for \qquad \sigma_m(t) > 0 \tag{1}$$

When D_a reaches a critical value C_{cr}, final rupture occurs. The criterion *for preventing rupture* can be summarized as follows:

$$\begin{cases} if \quad \sigma_I\left(t = t^*\right) \geq \sigma_I^{treshold} \\ \int_{t^*}^{t} \hat{\sigma}_m\left(t'\right) dt' \leq C_{cr} \\ where \\ \hat{\sigma}_m(t) = \frac{1}{2}\left(\sigma_m(t) + \left|\sigma_m(t)\right|\right) \end{cases} \tag{2}$$

Note that $\hat{\sigma}_m(t) = \sigma_m(t)$ for $\sigma_m(t) > 0$ while $\hat{\sigma}_m(t) = 0$ for $\sigma_m(t) \leq 0$. The parameters $\sigma_I^{treshold}$ and C_{cr} are material properties which may depend on strain-rate, triaxiality,

temperature, load amplitude and load rate. These values vary with time during dynamic loading. In the case of time varying parameters Eqn. 2 may be written:

$$if \quad \sigma_I\left(t^*\right) \geq \sigma_I^{treshold}\left(t^*\right)$$

$$\int_{t^*}^{t} \frac{\hat{\sigma}_m\left(t'\right)}{C_{cr}\left(t'\right)} dt' \leq 1 \qquad (3)$$

In this work we have assumed constant values of the parameters $\sigma_I^{treshold}$ and C_{cr}, and evaluated Eqn. 2. The evaluation was done within a commercial finite element software [41] by application of a user-subroutine (VUSDFLD)[42].

Eqn. 2 might be considered as a modification of the Nikiphorovski-Shemyakin criterion [35], [36] for uniaxial tension, which writes: $\int_0^t \sigma\left(t'\right) dt' \leq C_{cr}$. The proposed criterion is 3D and adds a *threshold* parameter $\sigma_I^{treshold}$. The integral is evaluated only for time $t>t^*$. It also states clearly that the additive value to the integral for $t>t^*$ is zero if $\sigma_m(t) \leq 0$. Moreover the damage evaluation and the threshold criterion do not have to be of the same character. Here we use the maximum principal stress as a threshold criterion, while the damage is calculated by considering the hydrostatic stress. The integration time (t') is not limited to the range $t-\tau \leq t' \leq t$ but we assume that once damage initiates at time t = t*, it keeps growing as long as $\sigma_m(t) > 0$ until final rupture.

2.2 Relationship between the proposed criterion and the kinetic equation of damage

Eqn. 2 can also be generated from the kinetic equation of damage which was introduced by Kachanov [43], [44] and was also used to justify the Nikiphorovski-Shemyakin criterion [35], [36]. According to Kachanov [42], damage is characterized by a scalar $0 \leq \psi \leq 1$ which is called "continuity". Initially (no damage), $\psi = 1$, but as time goes on, ψ decreases. When ψ is small, the process of fracturing, which is distributed over the volume, becomes unstable, and large cracks nucleate. The final brittle rupture corresponds to $\psi = 0$. Localization is not considered here because this last stage before final rupture is short. A simplified kinetic equation of damage which agrees generally well with experimental results for metals subjected uniaxial tension has been proposed [44]:

$$\frac{\partial \psi}{\partial t} = -A\left(\frac{\sigma}{\psi}\right)^{n} \tag{4}$$

Where $A > 1$ and $n \geq 1$ are material constants, and σ is the maximal tensile stress at a considered point. The ratio $\frac{\sigma}{\psi}$ can be interpreted as a certain effective stress. The solution of Eq. (1) is:

$$\psi^{n+1} = -(n+1)\int_{0}^{t} A\sigma^{n} dt + c \tag{5}$$

From the initial condition where the continuity parameter is ψ=1, one obtains c = 1 and the solution is:

$$\psi^{n+1} = 1 - (n+1)\int_{0}^{t} A\sigma^{n} dt \tag{6}$$

Here we relax the uniaxial formulation and extend it by substitution of the 3D hydrostatic stress σ_m. In uniaxial tension, $\sigma = 3\sigma_m$ where $\sigma_m = \frac{\sigma_{ii}}{3}$, $i = 1 \cdots 3$ is the average hydrostatic pressure. Equation (6) can be rewritten as:

$$\psi^{n+1} = 1 - (n+1)A\int_{0}^{t} \left(3\sigma_m\right)^{n} dt \tag{7}$$

If σ_m is constant during loading, given that at final rupture ψ = 0, *the time for rupture* is given by:

$$t_r = \frac{1}{(n+1)A\left(3\sigma_m\right)^{n}} \tag{8}$$

The damage (D) is defined as $D = 1 - \psi$ and $0 \leq D \leq 1$, therefore using Eq. (7):

$$0 \leq 1 - \left[1 - (n+1)A\int_{0}^{t} \left(3\sigma_m\right)^{n} dt\right]^{\frac{1}{n+1}} \leq 1 \tag{9a}$$

Which can be simplified to:

$$0 \le (n+1)A\int_0^t \left(3\sigma_m\right)^n dt \le 1 \qquad (9b)$$

Meaning that in order to prevent final rupture, the following condition must be fulfilled:

$$\int_0^t \left(\sigma_m\right)^n dt \le \frac{1}{3^n (n+1)A} \qquad (10a)$$

Or (writing explicitly the time dependency):

$$\int_0^t \left(\sigma_m\left(t'\right)\right)^n dt' \le C_{cr} \qquad for \qquad \sigma_m(t) > 0 \qquad (10b)$$

Where C_{cr} is a material property.

For n = 1 Eqn. 10b is identical in essence to Eqn. 2 , although the limits of integration are different .

The reader will note the general resemblance to the above-mentioned criterion of Tuler and Butcher [37].

3. Numerical simulations of normal impact on PMMA plates by a long steel projectile.

The impact is modeled using the commercial finite element software Abaqus explicit [41]. A 3D nonlinear transient explicit analysis is used.

3.1 Geometry, assembly and material properties

3.1.1 *Projectile*

The ogive head projectile (Fig. 2a) is made of steel with a density $\rho = 7800 \frac{Kg}{m^3}$. Its diameter is d = 6 mm and it has a total length of L = 56 mm. The head is ogive with L_h = 9.75 mm. Its volume is 1.47×10^{-6} m^3 and it weight is 11.4 gr. A bi-linear elastic-plastic (Mises plasticity) material model is used [42]. The Young's modulus is E = 210 GPa, Poisson's ratio is ν=0.3, the yield stress is 1.5 GPa and the hardening

modulus is Ep = 792 MPa. No failure criterion was used because the projectile does not fail in our experiments.

3.1.2 *PMMA round plates*

The target is made of 5 PMMA simply contacting plates, as shown in Fig. 2a. Each plate, shown in Fig. 2b, has a thickness of h = 5 mm and a diameter of D = ~98 mm. An elastic-plastic material model with Drucker-Prager (DP) plasticity is used for the PMMA [35].

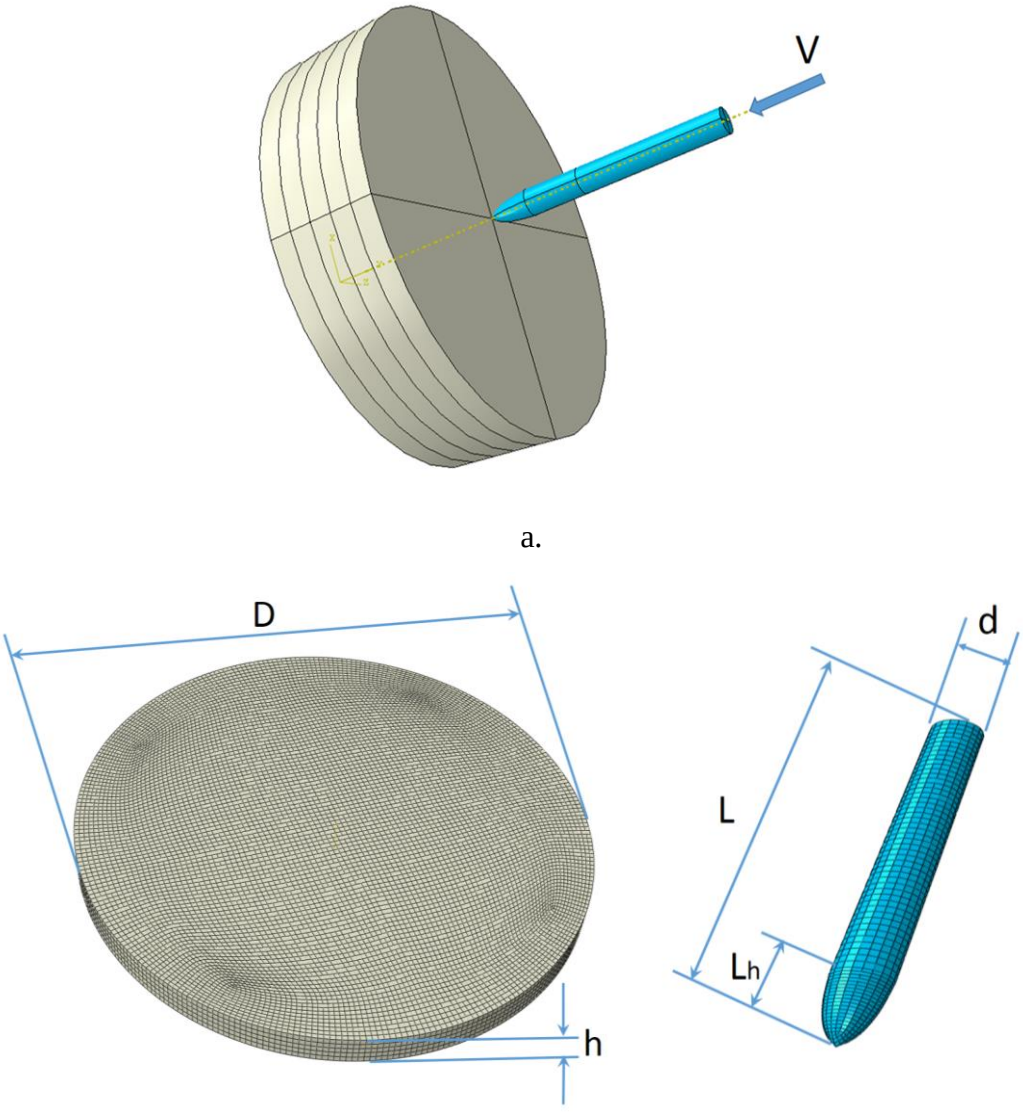

a.

b. c.

Figure 1: Assembly and parts. a. The assembly of the target made of 5 simply contacting plates and the projectile. b. A PMMA round plate with typical mesh. c. The meshed projectile.

The dynamic elastic modulus is E = 5.76 GPa, and Poisson's ratio is ν = 0.42[45]. The density is ρ = 1190 Kg/m^3 and the DP pressure sensitivity is β = 20^o [46], [47]. Experimentally determined uniaxial compression stress–plastic strain curves at different strain rates of: 0.0001, 1, 2000 and 4000 1/s are shown in Fig. 2, from [47]. In the absence of experimental data at significantly higher strain rates, we assumed that the behavior of the material is that measured at 4000 1/s. It is assumed that at extremely high strain rates, the strength of the material does not increase indefinitely.

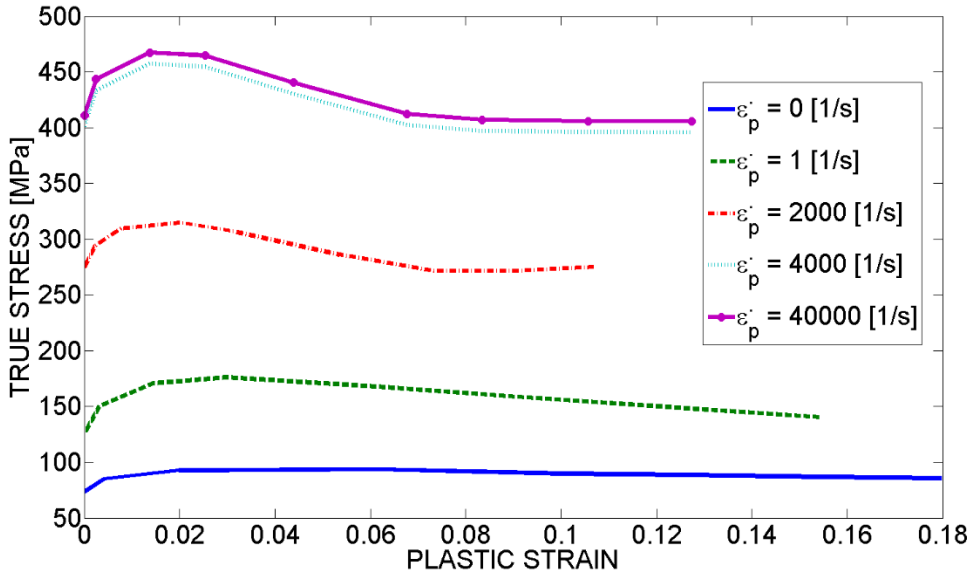

Figure 2: Experimentally determined uniaxial compression stress–plastic strain curves [46], [47] of PMMA at different strain rates of: 0.0001 , 1, 2000. 4000 and 40000 1/s.

At high strain rates, PMMA was shown to sustain reasonable plastic strains under confined compression, and fail by adiabatic shear banding [46] as opposed to brittle shattering in tension. Hence, two types of failure criteria were applied simultaneously:

1. Ductile damage with damage evolution [47] [42].
2. Tensile failure.

The plastic strains for failure at different strain rates and triaxiality levels are detailed in Table 1. The displacement damage evolution [42] was set to zero. The new brittle incubation time-based fracture criterion (Eqn. 2) is used, while in previous work [47] we used Abaqus tensile failure criterion [42] with a constant value. The threshold value of the maximum principal stress was taken to be 25 MPa while $60\ Pa\cdot s \le C_{cr} \ge 80\ Pa\cdot s$. Those values were found to yield a good agreement with experimental results that will be shown in the sequel.

Stain rate [1/s]	triaxiality			
	-0.6	-0.3	0	1
0.0001	0.68	0.3	0.02	0.01
1	0.6	0.24	0.0175	0.01
2000	0.44	0.22	0.01	0.0025
4000	0.4	0.2	0.0075	0.0015
40000	0.4	0.2	0.00075	0.0005

Table 1: Failure strains (ε_p^f) of PMMA versus triaxiality and strain rate. Those values were used in [47]for the negative triaxiality range, measured but not published for zero triaxiality, and were assumed for a triaxiality of 1.

3.2 Mesh and boundary conditions

The assembly of the 5 PMMA plates and the projectile at t = 0 are shown in Fig. 1a. The initial velocity of the projectile is V = 300 m/s. The general contact algorithm of Abaqus [42] is used with element-based surfaces which can adapt to the exposed surfaces of the current non-failed elements. All the surfaces that may become exposed during the analysis, including faces that are originally in the interior of bodies are included in the contact model. The contact domain includes the 5 PMMA plates and the projectile since the projectile trajectory is not known *a-priori*. Abaqus' frictional tangential behavior with the coefficient of friction f = 0.3 is adopted. The NODAL EROSION parameter is set to "NO" so contact nodes still take part in the contact calculations even after all of the surrounding elements have failed. These nodes act as free-floating point masses that can experience contact with the active contact faces.

A constant seed mesh size of 1 mm was used for the plates and projectile. Similar constant mesh size and structure were used in previous investigations [46]–[49]. One has to keep in mind that finite elements results which use erosion technique are mesh-sensitive. We studied in detail the mesh sensitivity in [46-49] and present only results for the optimal mesh. A typical structured mesh of the first plate is shown in Fig. 1b. A total number of 45600 linear hexahedral elements of type C3D8R are used. The mesh of the projectile is shown in Fig. 1c. The mesh seed along edges of the ogive head of

the projectile were downsized to 0.5 mm. A total number of 2928 linear hexahedral elements of type C3D8R are used

4. Experimental normal impact on PMMA plates by a long steel projectile.

An aluminum sabot is used to accelerate the projectile in a 6m long vacuumed barrel using the discharge of a 3L tank filled with compressed air (~30 bar). The impact takes place in a vacuumed chamber at the end of the barrel (~ 0.2 bar). A sabot stripper within the chamber is used to strip the projectile. A fast camera (KIRANA) is used to picture the impact event through the transparent wall of the chamber.

Four test were conducted. The impact velocity V_{in}, the outgoing velocity V_{out}, and the difference of the velocities $\Delta V = V_{in} - V_{out}$ are summarized in table 2.

Test number	V_{in} [m/s]	V_{out} [m/s]	ΔV [m/s]
1	282	229	53
2	302	224	78
3	301	224	77
4	318	251	67

Table 2: Velocity test results.

5. *Comparison of experimental and numerical results*

The experimental results show that an average impact velocity of 300.8±18 m/s was used. The resulting average outgoing velocity is 232±19 m/s which corresponds to an average velocity drop 69±16 m/s.

Figure 3 shows the numerically obtained velocity due to usage of three critical values: C_{cr} = 60, 70 and 80 Pa*s. The calculated exit velocity are 245, 232 and 225 m/s correspondingly. The black line represent the averaged experimental exit velocity. According to the variation of the impact and exit velocity (232±19 m/s) and Fig. 3 it can be estimated that the critical value is C_{cr} = 70 ±10 Pa*s.

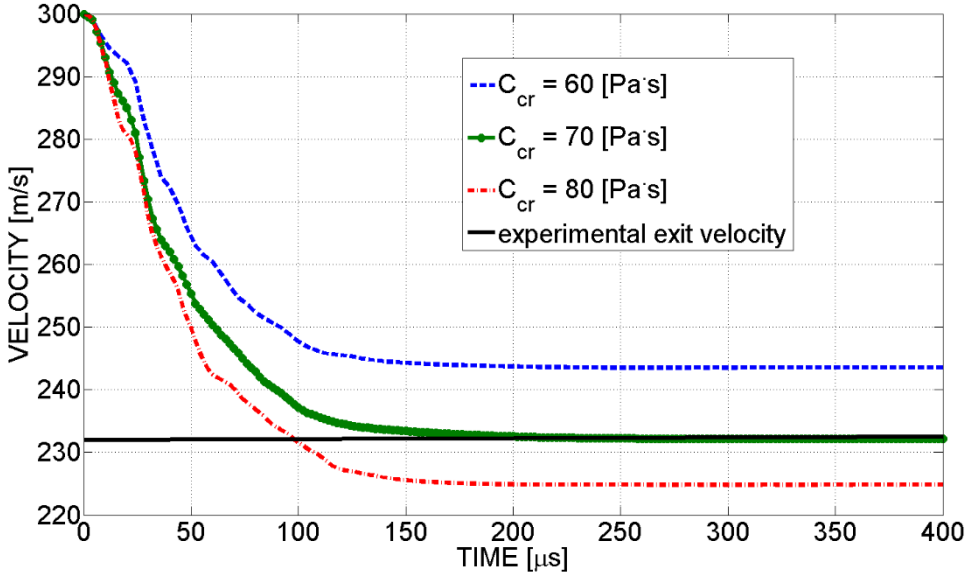

Figure 3: Numerically calculated velocity of the projectile. The asymptotic value at large times corresponds to the average projectile exit velocity

Figure 4 shows a comparison between the experimental video recording of test 2 and the numerical analysis for time intervals of 0, 50, 105, 130, 175, 210, 270, 320 and 400 μs, respectively. At 400 μs, the projectile has fully exited the target and travels at a constant velocity. One has to note that in the numerical analysis the failed elements are removed, while in reality they do not disappear. It should also be noted that at t = 0 μs, there is only a small amount of air in the chamber, but with time, more air/wind from the barrel enters the chamber and affect the flight of the fragments and shreds. Hence, a perfect agreement between the numerical and experimental pictures cannot be achieved.

Fig. 4. Shows the experimental and the numerical results side by side, illustrating the excellent agreement. The analysis predict the initial creation and growth of radial cracks in the first 150 μs or so, followed later by circumferential cracking (dishing) that tears the whole center of the plates. In addition, one can notice the development of short superficial crack segments from about 130 μs which are captured by the numerical simulations.

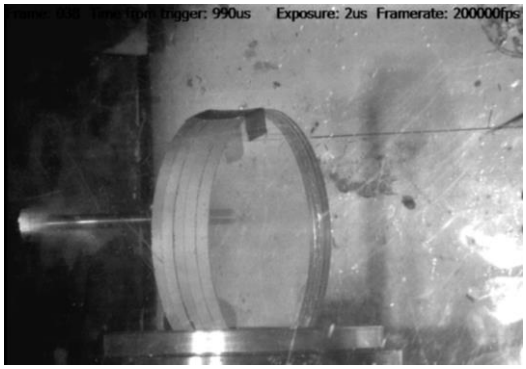

t = 0 µs

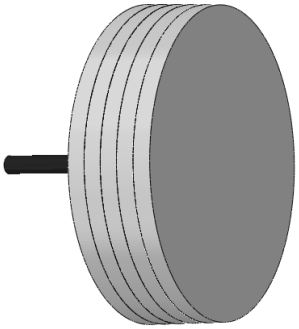

t = 0 µs

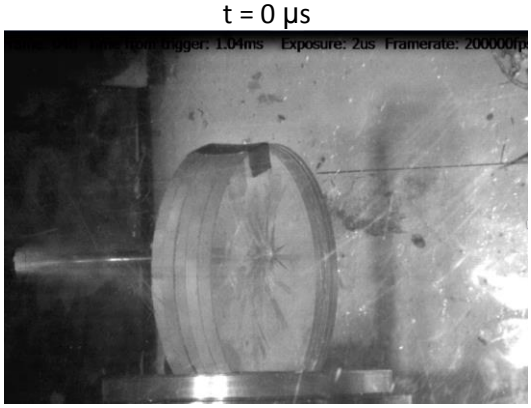

t=50 µs

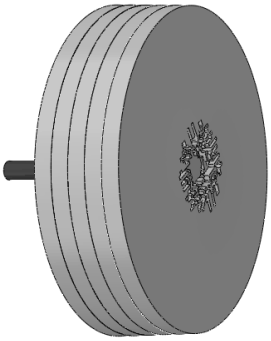

t=48 µs

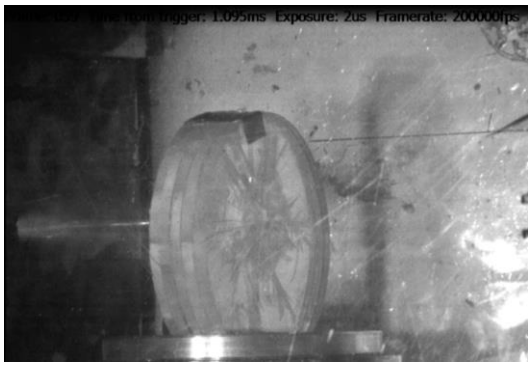

t=105 µs

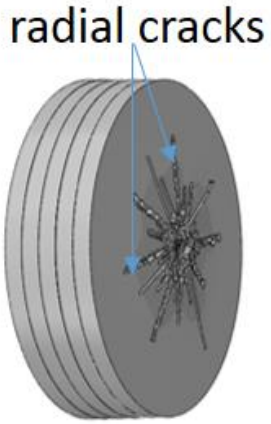

t=104 µs

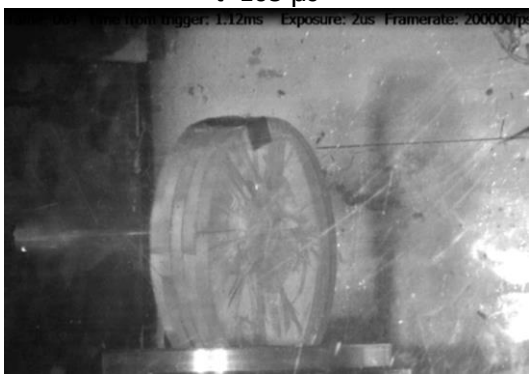

t = 130 µs

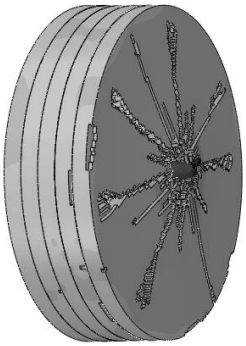

t = 128 µs

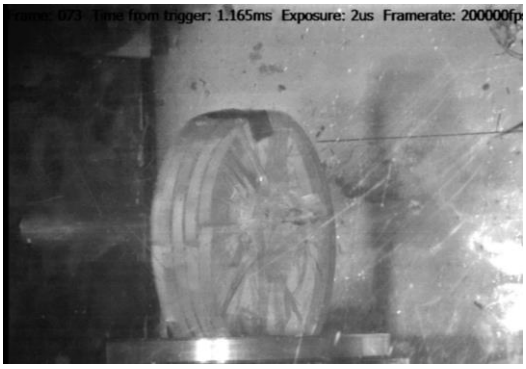

t = 175 µs

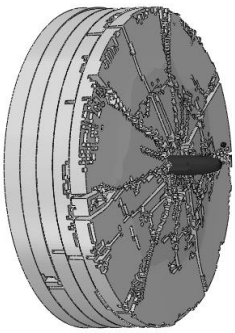

t = 174 µs

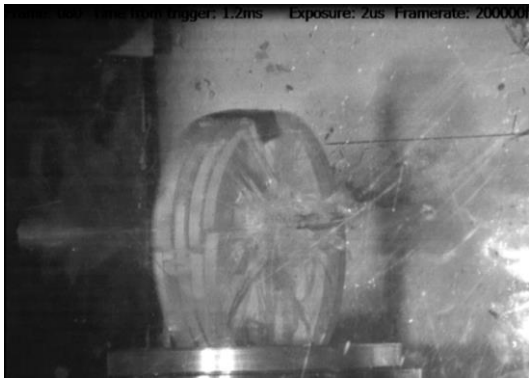

t = 210 µs

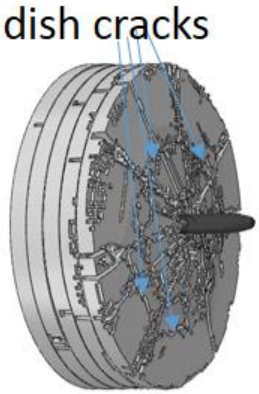

t = 208 µs

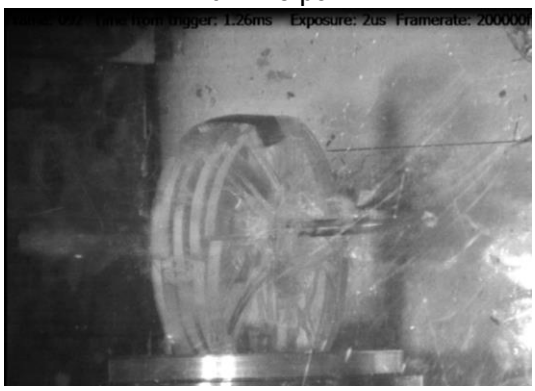

t = 270 µs

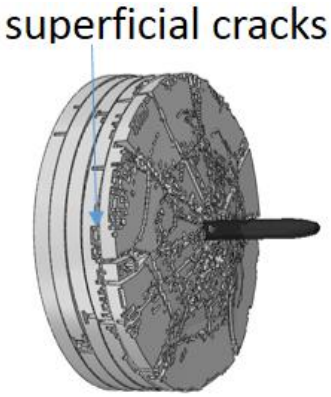

t = 272 µs

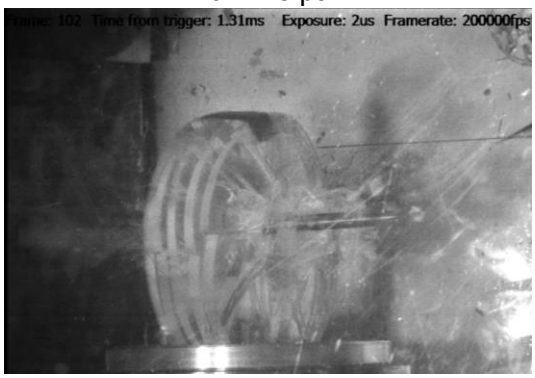

t = 320 µs

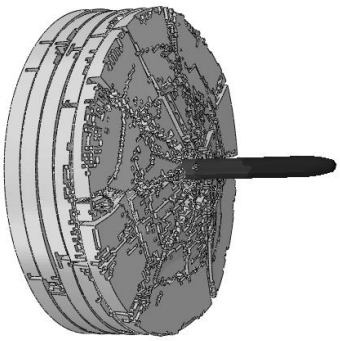

t = 320 µs

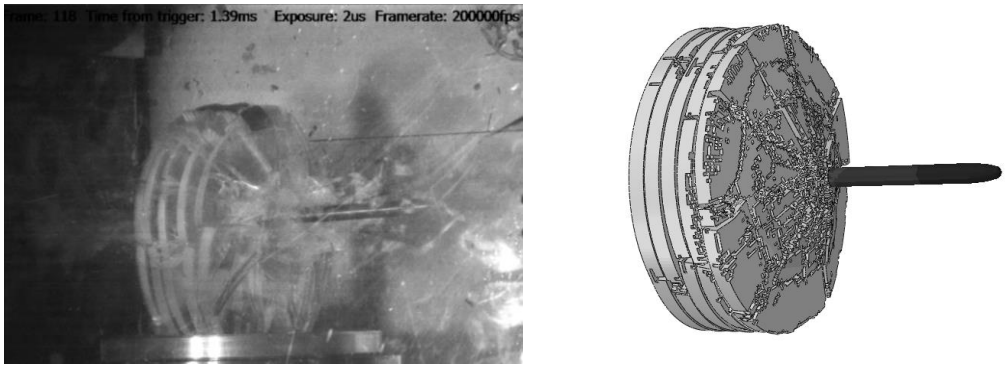

Figure 4: Experimental and numerical results for time intervals of 0, 50, 105, 130, 175, 210, 270, 320 and 400 μs. The experimental results are on the left side.

6. Summary and conclusions

A new dynamic brittle fracture criterion based on the time incubation concept was developed and implemented numerically to model ballistic penetration of 5 PMMA plates, as an example of brittle material. The comparison between the experimental and the numerical results showed that the exit velocity of the projectile was faithfully calculated, while the visual appearance of the fracture pattern, including its minute details, are quite resembling to the physical reality.

The present criterion presents a very simple alternative to the current strategies employed to model this kind of problems with results of a no lesser quality. As such, it is believed that the approach presented here should be enticing to the engineering community who needs simple tools to solve complex dynamic design problems.

Acknowledgement

The support of Maymad program (grant 2022734) is gratefully acknowledged.

Bibliography

[1] Z. Rosenberg and E. Dekel, “Asymmetric Interactions,” in *Terminal Ballistics*, Singapore: Springer Singapore, 2016, pp. 287–339.

[2] G. T. Camacho and M. Ortiz, “Computational modelling of impact damage in brittle materials,” *Int. J. Solids Struct.*, vol. 33, no. 20, pp. 2899–2938, Aug. 1996.

[3] R. Radovitzky, A. Seagraves, M. Tupek, and L. Noels, “A scalable 3D fracture and fragmentation algorithm based on a hybrid, discontinuous Galerkin, cohesive element method,” *Comput. Methods Appl. Mech. Eng.*, vol. 200, no. 1–4, pp. 326–344, Jan. 2011.

[4] J. Molinari, G. Gazonas, and R. Raghupathy, “The cohesive element approach to dynamic fragmentation: the question of energy convergence,” *Int. J.*, 2007.

[5] T. Rabczuk and T. Belytschko, “Cracking particles: A simplified meshfree method for arbitrary evolving cracks,” *Int. J. Numer. Methods Eng.*, vol. 61, no. 13, pp. 2316–2343, Dec. 2004.

[6] T. Belytschko, Y. Krongauz, D. Organ, M. Fleming, and P. Krysl, “Meshless methods: An overview and recent developments,” *Comput. Methods Appl. Mech. Eng.*, vol. 139, no. 1, pp. 3–47, Dec. 1996.

[7] M. B. Liu and G. R. Liu, “Smoothed Particle Hydrodynamics (SPH): an Overview and Recent Developments,” *Arch. Comput. Methods Eng.*, vol. 17, no. 1, pp. 25–76, Mar. 2010.

[8] X. Lai, B. Ren, H. Fan, S. Li, C. T. Wu, R. A. Regueiro, and L. Liu, “Peridynamics simulations of geomaterial fragmentation by impulse loads,” *Int. J. Numer. Anal. Methods Geomech.*, vol. 39, no. 12, pp. 1304–1330, Aug. 2015.

[9] H. Ren, X. Zhuang, Y. Cai, and T. Rabczuk, “Dual-horizon peridynamics,” *Int. J. Numer. Methods Eng.*, vol. 108, no. 12, pp. 1451–1476, Dec. 2016.

[10] G. Johnson and W. Cook, “Fracture characteristics of three metals subjected to various strains, strain rates, temperatures and pressures,” *Eng. Fract. Mech.*, 1985.

[11] G. Johnson and W. Cook, “A constitutive model and data for metals subjected to large strains, high strain rates and high temperatures,” *7th Int. Symp. ...*, 1983.

[12] T. Holmquist and G. Johnson, “Characterization and evaluation of silicon carbide for high-velocity impact,” *J. Appl. Phys.*, 2005.

[13] T. Holmquist and G. Johnson, “Characterization and evaluation of boron carbide for plate-impact conditions,” *J. Appl. Phys.*, 2006.

[14] T. Holmquist and G. Johnson, “Response of boron carbide subjected to high-velocity impact,” *Int. J. Impact Eng.*, 2008.

[15] T. Holmquist and G. Johnson, “A computational constitutive model for glass subjected to large strains, high strain rates and high pressures,” *J.*, 2011.

[16] T. Børvik, M. Langseth, O. S. Hopperstad, and K. A. Malo, “Ballistic penetration of steel plates,” *Int. J. Impact Eng.*, vol. 22, no. 9–10, pp. 855–886, Oct. 1999.

[17] T. Borvik, M. Langseth, O. S. Hopperstad, and K. A. Malo, “Perforation of 12mm thick steel plates by 20mm diameter projectiles with flat, hemispherical and conical noses - Part I: Experimental study,” *Int. J. Impact Eng.*, vol. 27, no. 1, pp. 19–35, Jan. 2001.

[18] A. Rusinek, J. A. Rodríguez-Martínez, R. Zaera, J. R. Klepaczko, A. Arias, and C. Sauvelet, “Experimental and numerical study on the perforation process of mild steel sheets subjected to perpendicular impact by hemispherical projectiles,” *Int. J. Impact Eng.*, vol. 36, no. 4, pp. 565–587, 2009.

[19] A. Rusinek and R. Zaera, “Finite element simulation of steel ring fragmentation under radial expansion,” *Int. J. Impact Eng.*, 2007.

[20] T. C. P. Analysis, M. Ortiz, and A. Pandolfi, “Finite-Deformation Irreversible Cohesive Elements for Three-Dimensional Crack-Propagation Analysis,” *Int. J. Numer. Meth. Engng*, vol. 44, pp. 1267–1282, 2000.

[21] E. Repetto, R. Radovitzky, and M. Ortiz, “Finite element simulation of dynamic fracture and fragmentation of glass rods,” *Comput. Methods Appl. Mech. Eng.*, vol. 183, pp. 3–14, 2000.

[22] F. Zhou, J. F. Molinari, and K. T. Ramesh, “A cohesive model based fragmentation analysis: Effects of strain rate and initial defects distribution,” *Int. J. Solids Struct.*, vol. 42, no. 18–19, pp. 5181–5207, 2005.

[23] F. Zhou and J. F. Molinari, “Dynamic crack propagation with cohesive elements: a methodolgy to address mesh dependence,” *Int. J. Numer. Methods Eng.*, vol. 59, no. 1, pp. 1–24, 2004.

[24] F. Zhou and J. F. Molinari, “Stochastic fracture of ceramics under dynamic tensile loading,” *Int. J. Solids Struct.*, vol. 41, no. 22–23, pp. 6573–6596, 2004.

[25] J. F. Molinari, G. Gazonas, R. Raghupathy, A. Rusinek, and F. Zhou, “The cohesive element approach to dynamic fragmentation: the question of energy convergence,” *Int. J. Numer. Methods Eng.*, vol. 69, no. 3, pp. 484–503, Jan. 2007.

[26] F. Zhou and J.-F. Molinari, “Stochastic fracture of ceramics under dynamic tensile loading,” *Int. J. Solids Struct.*, vol. 41, no. 22–23, pp. 6573–6596, Nov. 2004.

[27] F. Zhou and J. F. Molinari, “Dynamic crack propagation with cohesive elements: a methodology to address mesh dependency,” *Int. J. Numer. Methods Eng.*, vol. 59, no. 1, pp. 1–24, Jan. 2004.

[28] F. Zhou, J.-F. Molinari, and K. T. Ramesh, “A cohesive model based fragmentation analysis: effects of strain rate and initial defects distribution,” *Int. J. Solids Struct.*, vol. 42, no. 18–19, pp. 5181–5207, Sep. 2005.

[29] E. A. Repetto, R. Radovitzky, and M. Ortiz, “Finite element simulation of dynamic fracture and fragmentation of glass rods,” *Comput. Methods Appl. Mech. Eng.*, vol. 183, no. 1–2, pp. 3–14, Mar. 2000.

[30] M. Ortiz and A. Pandolfi, “Finite-deformation irreversible cohesive elements for three-dimensional crack-propagation analysis,” *Int. J. Numer. Methods Eng.*, vol. 44, no. 9, pp. 1267–1282, Mar. 1999.

[31] G. T. Camacho and M. Ortiz, “Computational modelling of impact damage in brittle materials,” *Int. J. Solids Struct.*, vol. 33, no. 20–22, pp. 2899–2938, Aug. 1996.

[32] F. Hild, C. Denoual, P. Forquin, and X. Brajer, “On the probabilistic-deterministic transition involved in a fragmentation process of brittle materials,” *Comput. Struct.*, vol. 81, no. 12, pp. 1241–1253, 2003.

[33] C. Denoual and F. Hild, “A Damage Model for the Dynamic Fragmentation of Brittle Solids,” *Comp. Meth. Appl. Mech. Eng.*, vol. 183, pp. 247–258, 2000.

[34] J. F. Kalthoff and D. A. Shockey, “Instability of cracks under impulse loads,” *J. Appl. Phys.*, vol. 48, no. 3, pp. 986–993, 1977.

[35] N. Morozov and Y. Petrov, *Dynamics of fracture*. 2013.

[36] V. Bratov, N. Morozov, and Y. V. Petrov, *Dynamic Strength of Continuum*. 2009.

[37] F. Tuler and B. Butcher, “A criterion for the time dependence of dynamic fracture,” *Int. J. Fract. Mech.*, vol. 4, no. 4, pp. 431–437, Dec. 1968.

[38] N. F. Morozov and Y. V Petrov, “Incubation time based testing of materials,” *Eur. J. Mech. A/Solids*, vol. 25, pp. 670–676, 2006.

[39] Y. V. Petrov and N. F. Morozov, “On the Modeling of Fracture of Brittle Solids,” *J. Appl. Mech.*, vol. 61, no. 3, p. 710, Sep. 1994.

[40] Y. V. Petrov, N. F. Morozov, and V. I. Smirnov, “Structural macromechanics approach in dynamics of fracture,” *Fatigue Fract. Eng. Mater. Struct.*, vol. 26, no. 4, pp. 363–372, Apr. 2003.

[41] Simulia, “Abaqus/CAE version 6.14-2 (2014). Dassault Systèmes Simulia Corp., Providence, RI, USA.” 2014.

[42] Simulia, “Abaqus/Explicit Version 6.14-2, Abaqus documentation . Dassault systemes, 2014.” 2014.

[43] L. M. Kachanov, “Introduction_to_Continuum_Damage_Mechanics,” *Journal of Applied Mechanics*. p. 135, 1990.

[44] L. M. Kachanov, “Rupture Time Under Creep Conditions,” *Int. J. Fract.*, vol. 97, no. 1/4, pp. 11–18, 1999.

[45] D. Rittel and H. Maigre, “An investigation of dynamic crack initiation in PMMA,” *Mech. Mater.*, vol. 23, pp. 229–239, 1996.

[46] D. Rittel and A. Brill, “Dynamic flow and failure of confined polymethylmethacrylate,” *J. Mech. Phys. Solids*, vol. 56, pp. 1401–1416, 2008.

[47] A. Dorogoy, D. Rittel, and A. Brill, “A study of inclined impact in polymethylmethacrylate plates,” *Int. J. Impact Eng.*, vol. 37, no. 3, pp. 285–294, 2010.

[48] A. Dorogoy and D. Rittel, “Effect of confinement on thick polycarbonate plates impacted by long and AP projectiles,” *Int. J. Impact Eng.*, 2015.

[49] D. Rittel and A. Dorogoy, “Impact of thick PMMA plates by long projectiles at low velocities. Part I: Effect of head’s shape,” *Mech. Mater.*, vol. 70, pp. 41–52, 2014.